Environmental Science Advances

ROYAL SOCIETY OF CHEMISTRY

PAPER

View Article Online
View Journal | View Issue

Cite this: *Environ. Sci.: Adv.*, 2025, **4**, 1767

Lithium nickel manganese cobalt oxide particles cause developmental neurotoxicity in *Caenorhabditis elegans*

Roi Faroud Lopez, † Javier Huayta, † Gordon D. Z. Williams, Sarah A. Seay, Pooja D. Lalwani, Sasha N. Bacot, Avner Vengosh and Joel N. Meyer*

Lithium is increasingly used in rechargeable batteries for mobile devices, electric vehicles, and energy storage, among other applications. One of the common formulations of lithium batteries is lithium nickel manganese cobalt oxide (LiNMC) particles. Increasing utilization of LiNMC batteries would require adequate disposal and/or recycling, and yet the potential disposal of lithium batteries as waste either in or outside of landfills might lead to toxic effects to people and wildlife. However, understanding of the potential toxicity of LiNMC particles is limited. Based on previous literature investigating the mechanisms of toxicity of the constituent metals, as well as lithium cobalt oxide (LCO) nanoparticles, we hypothesized that LiNMCs would cause toxicity *via* mitochondrial impairment and oxidative stress. We further hypothesized that LiNMC toxicity would be exacerbated by knockdown of *frh-1* and *gas-1*, *Caenorhabditis elegans* orthologs of human mitochondrial disease genes frataxin and NDUFS2. Finally, we predicted that LiNMC exposure would cause developmental neurotoxicity. We tested these predictions by carrying out LiNMC exposures, and found these did not significantly impact the redox state, steady-state ATP levels, mitochondrial:nuclear DNA ratio, or oxygen consumption in worms exposed developmentally to amounts of LiNMC that caused mild growth inhibition. We discuss possible reasons for the difference between our results and previous publications, including particle size. Furthermore, while knockdown of *frh-1* and *gas-1* altered several parameters, knockdown of these genes did not increase or decrease the effects of LiNMCs. However, we did find that exposure to LiNMC caused degeneration of dopaminergic, cholinergic, glutamatergic, and GABAergic neurons, but not serotonergic neurons or glial cells. Interestingly, it appears that the developmental neurotoxicity was driven either by a particle-specific effect, or a component other than lithium, because exposure to lithium chloride at the same concentration had no effect.

Received 17th April 2025
Accepted 24th September 2025

DOI: 10.1039/d5va00103j

rsc.li/esadvances

Environmental significance

LiNMC particles are prevalent in rechargeable batteries widely used in electric vehicles and other electronic devices. There is very limited recycling of these materials, and concern exists for human and ecological health impacts after disposal. A particular concern is developmental neurotoxicity, because many of the individual elements present in LiNMCs are developmental neurotoxicants, but there is little literature on the developmental neurotoxicity posed by LiNMCs. We evaluated the effects of developmental exposure to LiNMC particles on developmental neurotoxicity and mitochondrial function in *C. elegans*. The most striking effects that we observed were that parental exposure to LiNMC particles leads to developmental neurotoxicity of dopaminergic, glutamatergic, cholinergic, and GABAergic neurons in offspring.

1 Introduction

Lithium (Li) is commonly and increasingly used in batteries in electrical vehicles,[1] energy storage, and other electronics, because it can store a large amount of energy per unit weight, improving the battery's ability to store and deliver energy.[2] In recent years, lithium has been increasingly utilized through mixing with transition metals, including manganese (Mn), cobalt (Co), and nickel (Ni), in the cathode of the battery, creating lithium cobalt oxide (LCO) and, more recently, LiNMC batteries. This metal mixture creates a high energy density cathode, resulting in an efficient battery.[3] Along with these benefits, there is concern that production and use of lithium-containing batteries may affect human and environmental health. Lithium mining and battery production can cause significant lithium release into the environment, and release

Nicholas School of the Environment, Duke University, Durham, NC, USA. E-mail: joel.meyer@duke.edu

† These authors contributed equally to this work.

also occurs during LiNMC battery use and recycling.[4–7] However, few lithium batteries are in fact recycled (~5% in 2020 (ref. 8)), and batteries can pollute the environment through leaching into soil and groundwater after disposal in landfills or elsewhere (Fig. 1A). Upon disposal to the environment, leachates originating from weathering of disposed LiNMC battery can carry heavy metals in particulate form[9] with documented ecotoxicity.[10] They can also contribute to fires that may result in formation and distribution of airborne particles; about 25% of total landfill fires in the UK in 2017–2018 were due to discarded lithium batteries. Such fires produce smoke containing many toxic components[9] that are detrimental to human health.

The toxicities of the individual metal components of LiNMCs have been relatively extensively researched. Lithium is commonly prescribed clinically for mental health, including bipolar disorder.[11] It has a narrow therapeutic index, however, and excessive levels in acute or chronic exposure can cause effects including neurotoxicity and kidney toxicity.[12] There is particular concern about developmental exposures and developmental neurotoxicity, complicating risk–benefit considerations for the use of lithium in pregnancy.[13–16] Research into its mechanisms of toxicity has suggested an increase of oxidative stress[17] and mitochondrial dysfunction.[18] These mechanisms have also been proposed for nickel toxicity, which can ultimately lead to respiratory, cardiovascular, and kidney effects.[19–21] Irregular exposure to manganese, which can happen through mining and occupational use, is strongly associated with neurotoxicity.[22] Specifically, the biological manifestation of manganese toxicity is similar to Parkinson's disease.[23] Manganese in the body is concentrated in the mitochondria,[24] where it is a co-factor in numerous critical enzymes involved in metabolism,[25] and toxicity has been associated with mitochondrial dysfunction.[23] Finally, chronic and high cobalt exposure can lead to cardiac issues and thyroid complications,[26] also by affecting mitochondrial pathways and components.[27] Thus, each of the metals that compose LiNMC batteries has human health effects individually.

However, more limited research has been done specifically on lithium-mixture particles. A body of literature on LCO particles has led to proposed mitochondrial toxicity and oxidative stress mechanisms of action,[28–32] but fewer publications are available on LiNMC toxicity. Sharan *et al.* supports the generation of reactive oxygen species from LiNMC in *Shewanella oneidensis*, and links them to subsequent bacterial filamentation, DNA damage, and possibly DNA mutations.[33] Interestingly, Mitchell *et al.* states that bacterial damage from engineered nanomaterials producing reactive oxygen species can be repaired by reductases that reduce Cys and Met residues, SOS response, and mutS systems.[34] Bacteria can produce a biofilm that sequesters engineered nanomaterials to reduce bioavailability and later toxicity, and bacteria can sequester damaged DNA to prevent transmission to progeny. Hang *et al.* reported that metal ions from LiNMC decreased respiration and growth of soil bacteria.[35] Exposure of *Daphnia magna* to LiNMC decreased survival and reproduction[28] in a manner that could not be attributed to external dissolution of individual metal

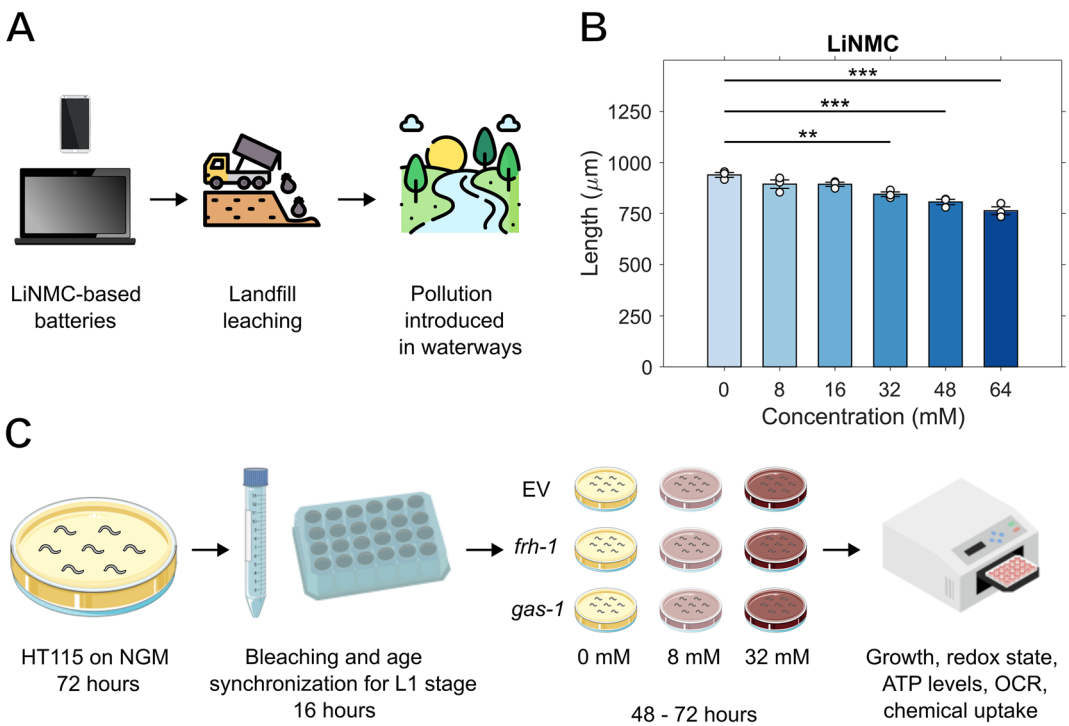

Fig. 1 Experimental concentrations and design. (A) Sources of LiNMC and potential introduction in the environment through landfill leaching. (B) Concentration-response of length measured at the L4 stage of worms exposed to LiNMC during development. (C) Schematic of experimental design. One-way ANOVA with Dunnet's test, error bars are SEM, $n = 3$ biological replicates (100 worms per treatment), (**) $p < 0.01$, (***) $p < 0.001$.

ions, potentially in part by inhibiting nutrient uptake. Niemuth *et al.* reported that LiNMCs inhibited the growth, development, and hemoglobin production with potential disruption of iron–sulfur cluster assembly.[29] Wang *et al.*[36] found that exposure of mice to LiNMC by various routes led to systemic distribution and, in the case of oropharyngeal aspiration, immunological response.

Given the growing importance of the rechargeable battery market, more research is needed into the potential toxicity of LiNMCs. Given the literature on the toxicity of LiNMCs, LCOs, and the individual metal constituents of these particles, we hypothesized that exposure to LiNMCs would cause mitochondrial dysfunction, redox stress, and neurotoxicity. We tested these hypotheses by directly measuring these parameters in the nematode worm *Caenorhabditis elegans*, as well as by testing the effects of LiNMCs after knockdown of *frh-1* and *gas-1*, orthologs of two human mitochondrial disease genes, frataxin and NDUFS2. *frh-1* is important for iron–sulfur cluster assembly, such that its knockdown should affect the same pathway described by Niemuth *et al.*,[32] while *gas-1* is a critical component of Complex I of the mitochondrial electron transport chain. *gas-1* and *frh-1* mutant worms are oxidative stress-sensitive[37,38] and bioenergetically challenged,[39,40] again suggesting that worms with knockdown of these genes should be sensitive to LiNMC exposure if LiNMCs cause oxidative stress and mitochondrial dysfunction. The RNAi knockdown experiments were performed both to gain additional mechanistic insight (*i.e.*, would knockdown make the worms more sensitive to LiNMCs) and to provide insight into whether humans with mutations in these genes might be more sensitive to LiNMC toxicity.

In this study, we used *C. elegans* to test the hypotheses that exposure to LiNMCs (<500 nm diameter) would lead to mitochondrial dysfunction, redox stress, and neurotoxicity. *C. elegans* is an established model for human and environmental toxicology,[41] nanomaterial toxicity,[42] mitochondrial toxicity,[43] and neurotoxicity.[44] Given the concerns about potential developmental neurotoxicity of lithium and literature demonstrating LiNMC effects on growth, we carried out exposures during development. However, we intentionally chose exposure concentrations that led to only mild effects on growth, so that our mechanistic interpretations would not be confounded by generalized organismal toxicity. We did not find support for the hypothesis that LiNMCs would cause redox stress or bioenergetic alterations at the whole-organism level, but did find evidence of developmental neurotoxicity that could not be attributed to the lithium content of the LiNMCs. Finally, knockdown of *frh-1* and *gas-1* did not increase sensitivity to LiNMCs. The data obtained in this study furthers the body of knowledge on adverse effects and mechanism of toxicity of LiNMC particles, prevalent in rechargeable batteries widely found in electronic devices. Multiple elements that constitute LiNMC have been described to be developmental neurotoxicants, highlighting the importance of evaluating the potential effects of these chemicals on mitochondrial functions and neurodegeneration. Our findings in the simple model organism *C. elegans* should be motivation for additional research aimed at understanding whether environmental LiNMC exposure could contribute to developmental neurotoxicity and impact human and ecological health."

2 Materials and methods

2.1. *C. elegans* strains and maintenance

C. elegans strains N_2 (Bristol wildtype), JV2 (*jrIs2*[*rpl-17*p::Grx1-roGFP2 + *unc-119*(+)]), PE255 (*feIs5*[*sur-5*p::luciferase::GFP + *rol-6*(su1006)] X), BY200 (*vtIs1*[p*dat-1*::GFP]), DA1240 (*adIs1240* [*eat-4*::sGFP + *lin-15*(+)]), LX929 (*vsIs48*[*unc-17*::GFP]), CZ1632 (*juIs76*[*unc-25*p::GFP + *lin-15*(+)]), GR1366 (*mgIs42*[*tph-1*::GFP + *rol-6*(su1006)]), and VT1485 (*maIs188*[*mir-228*p::GFP + *unc-119*]) were maintained at 20 °C on K-agar plates[45] seeded with OP50 *E. coli*. All strains were obtained from the *Caenorhabditis* Genetics Center, which is funded by NIH Office of Research Infrastructure Programs (P40OD010440).

2.2. Exposure to LiNMC and RNAi on plates

The experiment preparations began by creating nematode growth medium (NGM) agar plates to be seeded with HTT15 (DE3) L4440 empty vector (negative control, control).[46] The NGM protocol was modified to include 10 mL of Nystatin (Fisher Scientific) solution (12.5 mg Nystatin in 10 mL ethanol) and 2 mL cholesterol in ethanol at 10 mg per mL per 2 L of Milli-Q Water System filtered water. The liquid feeding culture was prepared following the published protocol[47] except for 10 g of NaCl instead of 5 g, and 20 g of Difco Agar Bacteriological (Fisher Scientific) instead of 15 g per L of water were used for the LB agar. LB broth was also made according to the published protocol[46] except for using 10 g of NaCl instead of 5 g and without including 1 M NaOH in the solution. After 20 hours bacterial incubation period in Incu-Shaker 10 L, at 37 °C and 200 rpm, NGM feeding plates were seeded with 300 μL of HT115 culture.

For $LiNi_{0.33}Mn_{0.33}Co_{0.33}O_2$ (LiNMC; Sigma 761001; particle size <500 nm; 346417-97-8; purity >98%) and RNAi co-exposure, NGM with carbenicillin disodium (Sigma-Aldrich) and isopropyl-β-D-1-thiogalactopyranoside (IPTG, Sigma-Aldrich) concentrations of 100 μg mL^{-1} and 0.5 mM, respectively were created.[48] In this composition of LiNMC, Ni, Mn, and Co are present in equal amounts as Ni = 33%, Mn = 33%, and Co = 33%.

NGM plates were seeded and spiked with RNAi liquid culture and LiNMC at the same time. The distinct RNAi liquid cultures were for HTT15 (DE3) L4440 control, HTT15 (DE3) L4440 with *frh-1* sequence (Horizon Discovery), HTT15 (DE3) L4440 with *gas-1* sequence (Horizon Discovery), and HTT15 (DE3) L4440 with *unc-22* sequence for RNAi. The RNAi liquid culture with ampicillin at 100 μg mL^{-1} was reared according to published protocol.[48] After 20 hours incubation period, as previously described, the RNAi liquid stock was centrifuged at 3000 RCF for 10 minutes. After centrifugation, half of the supernatant was removed to double the bacterial concentration. The LiNMC suspension concentrations were created using Milli-Q Water System filtered water at 64 mM and 16 mM. Sonicated with

Q500 Sonicator (Qsonica) followed with total sonication time of 20 minutes with amplitude of 25% and on and off pulses of 10 seconds.

After sonication, plates were immediately seeded with 150 μL of each concentrated liquid RNAi bacterial culture and 150 μL of LiNMC. The bacterial liquid culture in the NGM plate diluted the LiNMC concentrations to 32 mM and 8 mM. There were 9 treatments in ATP, redox state, OCR experiments: control 0 mM, control 8 mM, control 32 mM, *frh-1* RNAi 0 mM, *frh-1* RNAi 8 mM, *frh-1* RNAi 32 mM, *gas-1* RNAi 0 mM, *gas-1* RNAi 8 mM, and *gas-1* RNAi 32 mM. NMG plates were seeded with *unc-22* KD liquid bacteria and LiNMC as a visual confirmation of RNAi effectiveness. Plates were left at room temperature for 48 hours for bacterial lawn growth.

Regarding exposure generations, adult populations from distinct worm strains (either JV2, PE255, or N2) raised in HT115 control NGM plates were bleached, and eggs were overnight synchronized for 16 hours to get L1s[49] with the following modifications: use of K medium and K^+ buffers and centrifugation at 2200 RCF. Also, the bleaching solution contained 10 mL of sodium hypochlorite solution (Sigma-Aldrich), five pellets of sodium hydroxide (Macron Fine Chemicals), and approximately 40 mL of Milli-Q Water System filtered water. To avoid starvation, adult Control and *frh-1* RNAi populations were transferred to new NGM HT115 plates and 24 hours after they were bleached and overnight synchronized. After overnight synchronization, worms were plated for a joint 48 hours exposure for control (no LiNMC) and *frh-1* RNAi and 72 hours exposure for *gas-1* RNAi treatments.

After the end of exposure, worms were analyzed for ATP, redox state, and OCR. Approximately 1800 worms were analyzed for each treatment per ATP biological replicate. Approximately 4000 worms per treatment were analyzed for redox state per biological replicate. Approximately 100–150 worms were analyzed for OCR per treatment and per biological replicate. Worms analyzed for ATP, redox state, and OCR experiments were also analyzed for differences in length resulting from the RNAi and LiNMC co-exposure.

2.3. Exposure to lithium compounds in liquid

N2 worm populations were raised in OP50 K Agar plates and when adult, bleached and their offspring were overnight synchronized, as described in previous section.[49] Worms were then transferred to a 24-well plate and exposed for 48 hours to 250 μL per well of lithium chloride (LiCl; Sigma L9650; 7447-41-8; purity ≥99%), lithium acetate dihydrate (LiAc; Sigma L6883; 6108-17-4; reagent grade), and LiNMC. The exposure concentrations for LiCl and LiAc were 0 μM, 250 μM, 500 μM, 1250 μM, 2500 μM, 5000 μM, and 10 000 μM. Exposure concentrations for LiNMC were 0 μM, 250 μM, 500 μM, 1000 μM, 1500 μM, 2000 μM, 4000 μM. Worms were provided with 100 μL per well of inactivated UVRA bacteria as a food source. ∼150 worms per well were exposed to the various lithium concentrations (1 well per lithium concentration). Once exposure initiated, the 24-well plates were placed on a shaking incubator at 20 °C. After the 48 hours lithium exposure, worms were analyzed for length. Three biological replicates were performed for LiCl and LiAc and two were done for LiNMC experiments.

2.4. Quantification of neurodegeneration

Worms were age-synchronized by treating a mixed adult population with sodium hypochlorite to dissolve the bodies of gravid adults and obtain their fertilized embryos as previously described.[46] These embryos were transferred to K^+ medium and allowed to hatch overnight. L1 larval stage worms were collected the next day and transferred to NGM plates seeded with HT115 *E. coli* and left for 48 hours to reach their L4 larval stage. These worms were transferred to new NGM plates containing HT115 *E. coli* and either 0, 8, or 32 mM LiNMC. After 24 hours, this parent population was collected by transferring the well content to a 15 mL conical tube. The volume was raised to 15 mL with K-medium. After allowing worms to settle for 5 minutes, the supernatant was vacuumed, and this washing step was repeated two more times. Worms were then suspended in 5 mL of K-medium containing final concentrations of 0.4 N sodium hydroxide and 20% v/v sodium hypochlorite to recover their embryos. These were transferred to NGM plates with HT115 *E. coli* for 52–54 hours to allow them to reach the L4 stage. At this point, L4 worms were washed three times and transferred to a 2% agarose pad on a glass slide. Z-stacks were acquired for individual worms' heads on a Keyence BZ-X710 microscope equipped with a Keyence BZ-X700E light-source and using a Nixon 40× (air) objective with 200 milliseconds of exposure with the 'high-sensitivity' option selected. Maximum projections of the Z-stacks were generated, and each dendrite of the cephalic neurons was scored with scoring systems as previously described.[50,51] Briefly, for dopaminergic neurons: 0 – no damage, 1 – irregular (curves), 2 – less than 5 blebs, 3 – 5 to 10 blebs, 4 – more than 10 blebs and/or breaks, 5 – breaks, 25 to 75% dendrite loss, and 6 – breaks, more than 75% dendrite loss. 0 – no damage, 1 – irregular (curves), 2 – 1 to 10 blebs, and 3 – more than 10 blebs and/or presence of breaks; for cholinergic neurons: 0 – no damage, 1 – irregular (curves), 2 – 1 to 10 blebs, and 3 – more than 10 blebs and/or presence of breaks; for glutamatergic neurons: 0 – no damage, 1 – 1 to 5 blebs, 2 – 6 to 10 blebs, and 3 – more than 10 blebs and/or presence of breaks; and for serotonergic neurons, GABAergic neurons and glial cells: 0 – no damage, and 1 – any type of damage. Statistical analysis was performed using the chi-squared test with Bonferroni correction of p values.

2.5. Determining working concentrations

A mixed adult worm population of strain N_2 was treated with sodium hypochlorite to recover the progeny and generate an age-synchronized population by overnight hatching as previously described. After 16 hours, L1 worms were transferred to NGM plates with HT115 *E. coli* containing approximately 100 L1 worms and either 0, 8, 16, 32, 48, or 64 mM LiNMC. After 48 hours, worms were collected and transferred to unseeded K-agar plates.[45] Plates containing worms were imaged using a Keyence BZ-X710 microscope using a Nikon 4× objective. Images were analyzed using the WormSizer add-in in ImageJ to

determine individual worm length of a minimum of 50 individuals.[52] Regression analysis to determine EC_{10} values for length was performed using MS Excel 365.

2.6. Quantification of chemical uptake

Frozen worms were freeze dried for 3 hours then transferred to 7 mL Savillex PFA screw top vials. Each sample was digested with 1 mL HNO_3 and 1 mL H_2O_2 (both Fisher Optima grade) on a hot plate at 115 °C for 12 hours. The digestion solution was then dried down at 100 °C and then redissolved with 0.5 mL HNO_3, 0.5 mL H_2O_2, and 1 mL deionized water (>18.0 MΩ cm^{-1}) at 115 °C for 6 hours. Trace elements in each solution were measured on an inductively coupled plasma mass spectrometer (ICP-MS, Thermo Fisher X-Series II), equipped with a collision/reaction cell and calibrated with NIST 1643e.

2.7. Quantification of redox state

Measuring roGFP (estimation of the GSSG/2GSH ratio) relied on loading worms into a 96-well white plate. There were four technical replicates per each of the nine treatments per biological replicate. There were approximately 1000 worms per technical replicate for all treatments in 100 μL of K-medium. The 96-well plate was inserted into the FLUOstar Optima (BMG LabTech) plate reader. Fluorescence was measured for two channels with gain adjustments. The first one had an excitation filter of 400–10 nm, representing oxidized GFP, and an emission filter of 520 nm. The second channel had an excitation filter of 485/12 nm, representing reduced GFP, and an emission filter of 520 nm. The fluorescence was measured, and the corrected oxidized GFP fluorescence over the corrected reduced GFP fluorescence was used to estimate glutathione redox change. The corrected oxidized and reduced GFP fluorescence was calculated by subtracting the fluorescence of blank wells containing K medium from the fluorescence of the well with worms.

2.8. Quantification of ATP

Measuring ATP relied on loading worms in a 96-well white plate. Each treatment per biological replicate had six technical replicate wells with approximately 300 worms per well in 100 μL of K-medium. After all the worms were loaded in the white plate, luminescence buffer solution was made in a 15 mL conical tube with 5.54 mL of 0.2 M dibasic sodium phosphate (Na_2HPO_4), 2.46 mL of 0.1 M citric acid, 80 μL of dimethyl sulfoxide (DMSO, Sigma-Aldrich) (100%), 80 μL 5% Triton-X 100, and 80 μL 10 mM D-luciferin salt (in water). This luminescence buffer is required for measuring the luminescence of the PE255 strain. The 96-well plate was inserted into the FLUOstar Optima (BMG LabTech) plate reader and follow ATP reading protocol according to Luz *et al.*.[53] Updates to Luz *et al.* (2016) were using K medium for blank wells. Corrected luminescence over GFP fluorescence factor was used as the *in vivo* measurement of ATP for the PE255 reporter strain. Corrected luminescence was derived by subtracting the average luminescence of blank K-Med wells from the treatment luminescence. The GFP fluorescence factor was derived by dividing the corrected GFP fluorescence per treatment well over the average corrected GFP fluorescence per treatment. The corrected GFP fluorescence was derived by subtracting the average GFP fluorescence of blank K-medium wells from the treatment GFP fluorescence.

2.9. Quantification of length

After measuring ATP, redox state, and oxygen consumption rate, reporter strain subpopulation, worms were imaged for length. At the end of LiCl, LiAc, and LiNMC's liquid exposures, worms were also imaged for length. Worms were placed in the BZ-X710 (Keyence) fluorescent microscope, and the BZ-X Viewer software for imaging was launched. The objective size chosen was 4×. Length was measured for the experiments' biological replicates mentioned in previous sections.

ImageJ was used to determine the size of each worm. Within ImageJ, a plugin named WormSizer (version 1.2.5) was used to determine the worm length.

2.10. Oxygen consumption rate measurements

We used a Seahorse XFe96 Extracellular Flux Analyzer (Agilent) to quantify oxygen consumption rate (OCR) in worms following published protocols.[54] Briefly, worms exposed to LiNMC and grown on *frh-1* or *gas-1* RNAi plates were transferred to a Seahorse microplate at a concentration of 20 worms per well. Basal oxygen consumption rate (OCR) measurements are taken before injection of either 25 μM final concentration of carbonyl cyanide 4-(trifluoromethoxy) phenylhydrazone (FCCP) to measure maximal oxygen consumption or 20 μM final concentration of *N*,*N*-dicyclohexylcarbodiimide (DCCD), to determine ATP-linked respiration. After the injection of either FCCP or DCCD, 14 measurements were performed before a final injection of 10 mM final concentration of sodium azide to inhibit mitochondrial respiration and determine the non-mitochondrial OCR. Final parameters calculated include basal mitochondrial OCR, maximal OCR, spare capacity, ATP-linked respiration, proton leak, and non-mitochondrial OCR. Seahorse experiments included 5 wells per treatment group (technical replicates) and 3 biological replicates. Seahorse experiments were normalized to worm volume, determined by imaging a subset (n > 50 worms) per group using the ImageJ plugin WormSizer,[52] to mitochondrial DNA (mtDNA) copy number, and to the ratio of mitochondrial DNA copy number to nuclear DNA copy number, determined as described in the following section.

2.11. Mitochondrial and nuclear copy number

6 L4 worms exposed to LiNMC and grown on *frh-1* or *gas-1* RNAi plates were picked into 90 μL of worm lysis buffer (25 mM tricine, pH 8; 80 mM potassium acetate; 11% w/v glycerol; 2.25% v/v DMSO, 1 mg mL^{-1} proteinase K in nuclease-free water), and stored at −80 °C. Samples were lysed at 65 °C for 1 hour, followed by proteinase K inactivation for 15 minutes at 95 °C, with the resulting lysate used as a template in real-time PCR experiments as previously described.[55] Briefly, Power Sybr Green PCR Master Mix (ThermoFisher Scientific) was used with 2 μL of lysate for the template. CT values were converted to copy

number using a standard curve with the pCR 2.1 plasmid containing the species-specific mitochondrial *nduo-1* gene fragment for mtDNA or the *cox-4* gene fragment for nuclear DNA. Copy number was then calculated per worm. PCR was run in 3 technical replicates and 3 biological replicates.

2.12. Survival after rotenone

After age-synchronization following the steps described in the previous sections, worms were transferred to NGM plates containing either HT115 with empty vector or *unc-22* RNAi vector and grown at 20 °C until reaching the L4 larval stage. At this point, worms were transferred to fresh plates containing the same type of RNAi and a final concentration of 25 mM rotenone (calculated based on the volume of agar in the plate). Worms were scored for survival after 24 and 48 hours. A worm was considered dead if it did not respond to light prodding with a small aluminum wire mounted on a pick. Worms that showed bagging or that crawled out of the agar were censored.

2.13. Statistical analysis

MATLAB R2023a (MATLAB 9.14) was used for all statistical testing and graph generation. Statistical tests and sample size are described in their corresponding figure legends.

3 Results and discussion

3.1. Assessment of the effects of lithium compounds on growth of *C. elegans*

To identify concentrations of LiNMC that would have relatively mild organism-level effects such that our mechanistic studies would be unlikely to be confounded by non-specific side effects of generalized toxicity, we exposed worms to increasing concentrations of LiNMC during development. We found a statistically significant difference in average length of worms exposed to 32 mM LiNMC and higher. We selected concentrations leading to a reduction of 5 and 10% in length, using an EC_5 of 8 mM and EC_{10} of 32 mM (Fig. 1B). We also tested the effects of lithium chloride, lithium acetate, and LiNMC in liquid culture. After 48 hours of liquid exposure, the average length was significantly different from the control only for the highest concentration tested of 10 mM lithium chloride and 10 mM lithium acetate, with no differences observed for LiNMC up to 4 mM (Fig. S1). For subsequent experiments, we focused on plate exposures instead of liquid exposures to minimize complications with uptake associated with clumping of LiNMCs in liquid culture and to facilitate RNAi experiments.

3.2. Chemical uptake of lithium, nickel, manganese, and cobalt in *C. elegans*

To compare effects in *C. elegans* to other species including humans, it is critical to measure internal concentrations, because internal concentrations are often much different than growth medium concentrations in *C. elegans*.[56] We therefore quantified the uptake of the components of LiNMC in wildtype (N_2) worms without gene knockdown, and in worms in which *frh-1* and *gas-1* were knocked down using RNA interference (Fig. 1C). As described in the Introduction, these strains were used both to gain mechanistic insight and to provide evidence about whether mutations in these genes could lead to greater LiNMC toxicity, which could be an important gene × environment interaction.

We analyzed each of these components separately and found significantly increased internal concentrations of lithium, nickel, manganese, and cobalt with increased LiNMC exposure concentration (Fig. 2A–D), as demonstrated by statistically significant main effects of LiNMC exposure for all four of the chemicals analyzed (Fig. 2E). We did not observe differences in concentrations of other elements that were analyzed, but report concentrations of sodium, magnesium, aluminum, phosphorus, potassium, calcium, iron, copper, selenium, and molybdenum, because we are aware of only limited reporting on elemental concentrations in *C. elegans* (Table S1). Concentrations were ~19–100-fold lower inside the worms than the target medium concentrations. However, RNAi knockdown did not affect metal content either across exposures ($p > 0.168$) or at specific exposures ($p > 0.275$) (Fig. 2E). People with lithium intoxication have been reported to show serum lithium levels over 1.2 mM,[57] similar to the maximum concentration we measured of 1.16 mM (Fig. 2A). Minor side-effects of lithium used in bipolar disorder patients have been reported in the 0.6–1.2 mM range, within the internal concentration range we measured. Hemodialysis treatment was necessary in patients with lithium poisoning with serum concentrations in the 1.4–9.6 mM range,[58] again just over the maximum concentration observed in this work. Nickel exposure in residents living close to a cement factory were quantified, with the subject group reporting dermatitis and nickel contents in blood between 3.2–18.0 μg L^{-1} with an average of 7.8 μg L^{-1}.[59] Another study was performed with workers at an electroplating plant who accidentally ingested nickel sulfate and chloride and who reported multiple symptoms of toxicity.[60] Their serum nickel levels were in the 12.8–1340 μg L^{-1} range with average 286 μg L^{-1}. In this case, these nickel concentrations leading to toxicity in humans are comparable or lower than the 80.2–26 594 μg L^{-1} range we measured in worms (Fig. 2B). Death after ingestion of a cylindrical battery was associated with manganese toxicity with concentrations of 75 μg L^{-1} in peripheral blood and 38 μg L^{-1} in cardiac blood.[61] Reports of chronic exposure to manganese in drinking water leading to manganese poisoning symptoms were quantified in the 17.4–38.2 μg L^{-1} (ref. 62) and 3.6–2300 μg L^{-1} (ref. 63) ranges. In contrast, worms exposed to LiNMC showed manganese concentrations between 4965–88 400 μg L^{-1} (Fig. 2C), which are three to four orders of magnitude higher than those reported for manganese poisoning in humans. However, previous reports on the effects of manganese exposure in *C. elegans* found deficits in lifespan, development, and reproduction after 48 hours exposure to 4473–11 928 μg L^{-1};[64] and decreased oxygen consumption and decreased survival after exposure to 1790 and 2684 μg L^{-1} respectively.[65] Interesting, the internal Mn concentration that we measured is nearly identical to that reported in another *C. elegans* paper, 6.8 mM (Fig. 5, assuming a worm volume of 2200 pL), at their highest exposure concentration of 150 mM.[66] Finally, tests

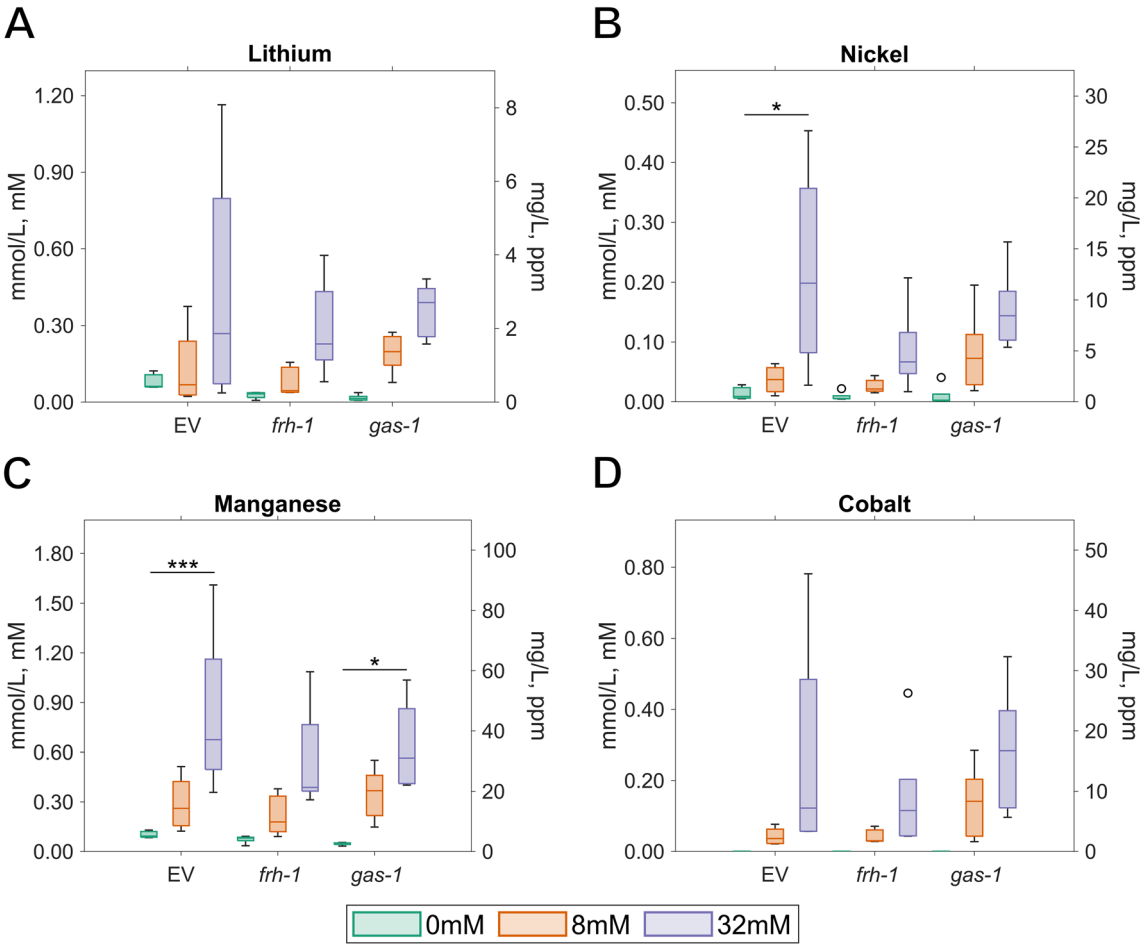

E

	Lithium	Nickel	Manganese	Cobalt
RNAi	0.541	0.168	0.457	0.384
LiNMC concentration	0.001	< 0.001	< 0.001	0.001
Interaction	0.907	0.275	0.758	0.778

Fig. 2 Chemical uptake of LiNMC. Internal concentrations in *C. elegans* of (A) lithium, (B) nickel, (C) manganese, and (D) cobalt in worms that were exposed to 0, 8, or 32 mM LiNMC, and EV, *frh-1*, or *gas-1* RNAi bacteria. Cobalt was not detected in unexposed worms. (E) Summary of the main effect and interaction *p*-value terms for RNAi and LiNMC concentration effects on chemical uptake in worms. Two-way ANOVA with Tukey-HSD test, $n = 5$ biological replicates (1050–2400 worms per treatment), asterisks in panels (A–D) indicate (*) $p < 0.05$ or (***) $p < 0.001$.

performed on metal workers determined cobalt blood levels of 5.7–7.9 μg L^{-1} and 59–78 μg L^{-1} in urine,[67] while a study where human volunteers ingested 1 mg per day cobalt for 90 days led to concentrations in blood of 6–117 μg L^{-1}[68] with neither study reporting health effects in their subjects. Our internal concentrations were higher by three to four orders of magnitude at 1248–46 060 μg L^{-1} of cobalt (Fig. 2D). These results indicate that although the concentrations of lithium we measured were lower than those considered harmful to humans, this was not the case for all three of the other chemicals present in LiNMC. With this consideration we proceeded to evaluate the effects of LiNMC exposure on indicators of mitochondrial health.

3.3. Redox state and ATP are not altered after exposure to LiNMC

Two-way ANOVA showed that there was a statistically significant effect of RNAi on the average length of the redox state reporter strain JV2 ($p = 0.032$ for main effect of RNAi) and a statistically significant decrease in average length with increasing LiNMC concentration ($p < 0.001$) (Fig. 3A). Size data is shown normalized to control conditions, because RNAi affected growth; non-normalized data are presented in SI Fig. 2. However, the effects of LiNMC on growth did not vary with RNAi treatment (interaction $p = 0.24$). For the control RNAi group, the 8 mM and 32 mM LiNMC treatments were significantly lower than the 0 mM treatment. For the *frh-1* RNAi group, only the 32 mM LiNMC treatment was significantly lower than the 0 mM

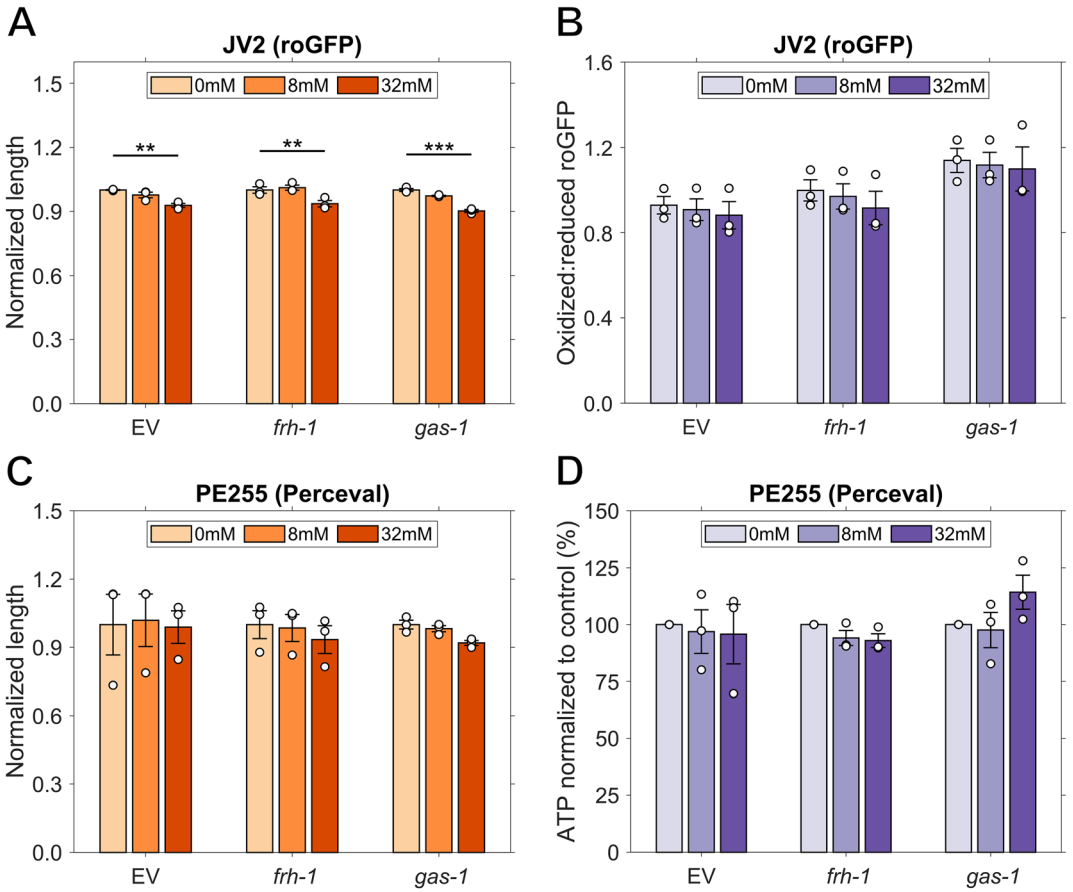

E

	JV2 length	oxi:red roGFP	PE255 length	norm. ATP
RNAi	0.032	0.002	0.818	0.305
LiNMC concentration	< 0.001	0.573	0.629	0.655
Interaction	0.241	0.997	0.992	0.478

Fig. 3 LiNMC exposure does not affect redox state or steady-state ATP levels in wild-type worms or after *gas-1* or *frh-1* knockdown. (A) JV2 length normalized to 0 mM LiNMC (B) redox state ratio (oxidized : reduced roGFP). (C) PE255 normalized length to 0 mM LiNMC. (D) ATP in percentage of control. (E) Summary of the main effects of RNAi and LiNMC concentration in chemical uptake in worms. Two-way ANOVA with Tukey-HSD test, $n = 3$ biological replicates for roGFP and Perceval quantification (12–18 technical replicates per 3 biological replicates, 300–1000 worms per technical replicate), $n = 3$ biological replicates for length determination (100 worms per treatment), error bars are SEM, (**) $p < 0.01$, (***) $p < 0.001$.

treatment. For the *gas-1* RNAi group, both the 8 mM and 32 mM LiNMC treatments were significantly lower than the 0 mM treatment. Interestingly, knockdown of neither *gas-1* nor *frh-1* sensitized to LiNMC treatment. In fact, while not statistically significant based on the interaction term, if anything, the *frh-1* RNAi knockdown was protective in the context of LiNMC exposure.

RNAi treatment had an effect on the redox state as assessed by the roGFP reporter in JV2 worms ($p = 0.001$ main effect), but LiNMC concentration had none ($p = 0.603$) (Fig. 3B). Further, the effect of RNAi treatment did not depend on the lithium concentration ($p = 0.998$ for interaction). Overall, *gas-1* RNAi presented a more-oxidized redox state compared to *frh-1* RNAi, and control worms (empty vector-fed). A caveat to this result is that the *gas-1* worms were slightly more developed than the *frh-1* and empty vector worms: *gas-1* worms develop more slowly (about 12 hours delay at 48 hours post-hatch), and were allowed an additional 24 hours, such that they were about 12 hours "older" than control and *frh-1*.

The ATP reporter strain was somewhat more resistant to growth inhibition by both RNAi ($p = 0.818$) and LiNMC concentration ($p = 0.629$) (Fig. 3C and S2). There was no interaction between RNAi and LiNMC exposure ($p = 0.992$). Similarly, neither RNAi nor LiNMC had an effect on steady-state ATP levels normalized to percent of lithium control (RNAi treatment main effect $p = 0.305$, LiNMC main effect $p = 0.655$; interaction term $p = 0.48$) (Fig. 3D and S3).

The main finding from these experiments was that LiNMC did not significantly affect redox state or steady-state ATP levels at concentrations that resulted in mild growth inhibition. A

secondary finding was that this was also true in the context of knockdown of *frh-1* and *gas-1*, and these knockdowns furthermore did not sensitize worms to growth inhibition by LiNMC. If LiNMC were causing toxicity by affecting mitochondrial bioenergetics or redox stress, we would expect that knockdown of these genes would sensitize worms to LiNMC exposure.

3.4. Exposure to LiNMC does not significantly alter oxygen consumption rate or mitochondrial DNA copy number

We considered the possibility that ATP levels in LiNMC-exposed worms might be sustained by increased non-mitochondrial energy production (*i.e.*, glycolysis), reduced energy expenditure, or other adaptive responses that could mask mitochondrial dysfunction as assessed by steady-state ATP levels. We therefore carried out a more detailed analysis of mitochondrial respiration as assessed by oxygen consumption without and with a variety of drugs that permit isolation of different aspects of mitochondrial function.[69] Oxygen consumption is a necessary part of the mitochondrial oxidative phosphorylation process, and dysfunction of aerobic mitochondrial bioenergetic processes can be assessed as changes in mitochondrial oxygen consumption rates in *C. elegans*.[54]

We found no effect of LiNMC on basal OCR ($p = 0.750$), but there was an effect of the RNAi being fed to the worms, with lower basal OCR regardless of LiNMC treatment in *gas-1* worms ($p = 0.021$) (Fig. 4A and H). Maximal OCR is quantified after uncoupling mitochondria causing mitochondria to consume oxygen at a maximal rate. We observed similar results to basal OCR with no effect from LiNMC concentration ($p = 0.236$) but an effect from RNAi ($p < 0.001$) (Fig. 4B and H). Spare capacity indicates the difference between maximal and basal OCR, and it shows the same effect of RNAi ($p < 0.001$) with no effect from LiNMC exposure ($p = 0.370$) but decreased spare capacity in *gas-1* worms (Fig. 4C and H). Mitochondrial basal OCR indicates the rate of oxygen consumed to convert ADP to ATP plus compensate for proton leak. We found this to follow the same pattern of a significant effect from RNAi feeding ($p = 0.002$) but not from LiNMC ($p = 0.883$) (Fig. 4D and H). Proton leak reflects the oxygen consumption in mitochondria after ATP synthase is blocked. Neither RNAi ($p = 0.114$) nor LiNMC ($p = 0.214$) had a significant effect on proton leak (Fig. 4E and H). Finally, non-mitochondrial OCR is associated with cellular processes outside of the electron transport chain that consume oxygen. RNAi type had a significant effect on non-mitochondrial OCR ($p = 0.005$), in this case being increased in *gas-1* worms, but LiNMC concentration did not have an effect ($p = 0.288$) (Fig. 4F and H). We quantified all of these oxygen consumption rates with two additional normalization approaches (Fig. S4). We found that normalization to mitochondrial DNA copy number (Fig. S4A–F) and the ratio of mitochondrial DNA copy number to nuclear DNA copy number (Fig. S4G–L) show the same trends described in this section. Although there were no significant effects of LiNMC concentration in the various types of OCR measured, there were significant effects of the type of RNAi fed to the worms. This expected given the fact that *gas-1* worms carry a defect in electron transport chain Complex I protein NDUFS2, and exhibit altered mitochondrial metabolism.[70]

Another potential indicator of mitochondrial health is mitochondrial DNA copy number. Environmental exposures can alter mtDNA copy number,[71–73] although not necessarily in a monotonic fashion.[74] We used a PCR based method to quantify the number of copies of both mitochondrial and nuclear DNA.[55,75] We found that neither LiNMC concentration ($p = 0.615$) nor RNAi type ($p = 0.214$) had a significant effect on the ratio of mtDNA to nDNA copy number (Fig. 4G and I). We observed the same lack of effect of LiNMC exposure on mtDNA copy number (Fig. S5A), nDNA copy number (Fig. S5B), or mtDNA copy number normalized to worm volume (Fig. S5C) to account for differences in development.

Finally, we characterized bioenergetics and rotenone resistance in worms fed *unc-22* RNAi (that were used for visual confirmation of the success of the RNAi protocol). We detected no differences in any oxygen consumption rate parameters, steady-state ATP, or mtDNA : nDNA ratio, but did find that *unc-22* knockdown resulted in a dramatic sensitization to rotenone (Fig. S6).

3.5. Parental exposure to LiNMC caused neuronal type-specific degeneration

All our assessments up to this point were at the whole-organism level. We next considered that there might be cell type-specific effects. Impaired mitochondrial function is strongly associated with neurodegeneration and neurons are considered to be particularly sensitive to mitochondrial dysfunction,[76] which led us to test for sensitivity of different neuronal populations to degeneration. We quantified neurodegeneration in multiple neuronal types (defined by neurotransmitter): dopaminergic, glutamatergic, cholinergic, GABAergic, and serotonergic, as well as glial cells, after parental exposure to LiNMC. Based on the concern for lithium exposure *via* exposure during pregnancy, we followed an approach we developed to simulate *in utero* exposure, with neurodegeneration evaluated in the progeny generation when it reached their final larval stage and all neuronal cells are fully formed.[51] For this purpose, we exposed the parent population to LiNMC for 24 hours, followed by recovering their embryos, allowing these to reach the L4 larval stage and imaging neurons located in their heads at this point (Fig. 5A).

We identified various types of morphological damage in dopaminergic, glutamatergic, cholinergic, and GABAergic neurons of progeny after LiNMC parental exposure (illustrative images in Fig. S7). We found statistically significant neurodegeneration after exposure to 8 and 32 mM LiNMC in dopaminergic and cholinergic neurons (Fig. 5B and D). We also found significant neurodegeneration in glutamatergic and GABAergic neurons (Fig. 5C and E), but only for the high concentration of 32 mM LiNMC. However, serotonergic neurons and glial cells did not exhibit significant degeneration with respect to their controls (Fig. 5F and G).

Next, we repeated the parental exposure for those neuronal types that we identified as affected by LiNMC exposure, but this time using lithium chloride at the same molar concentrations.

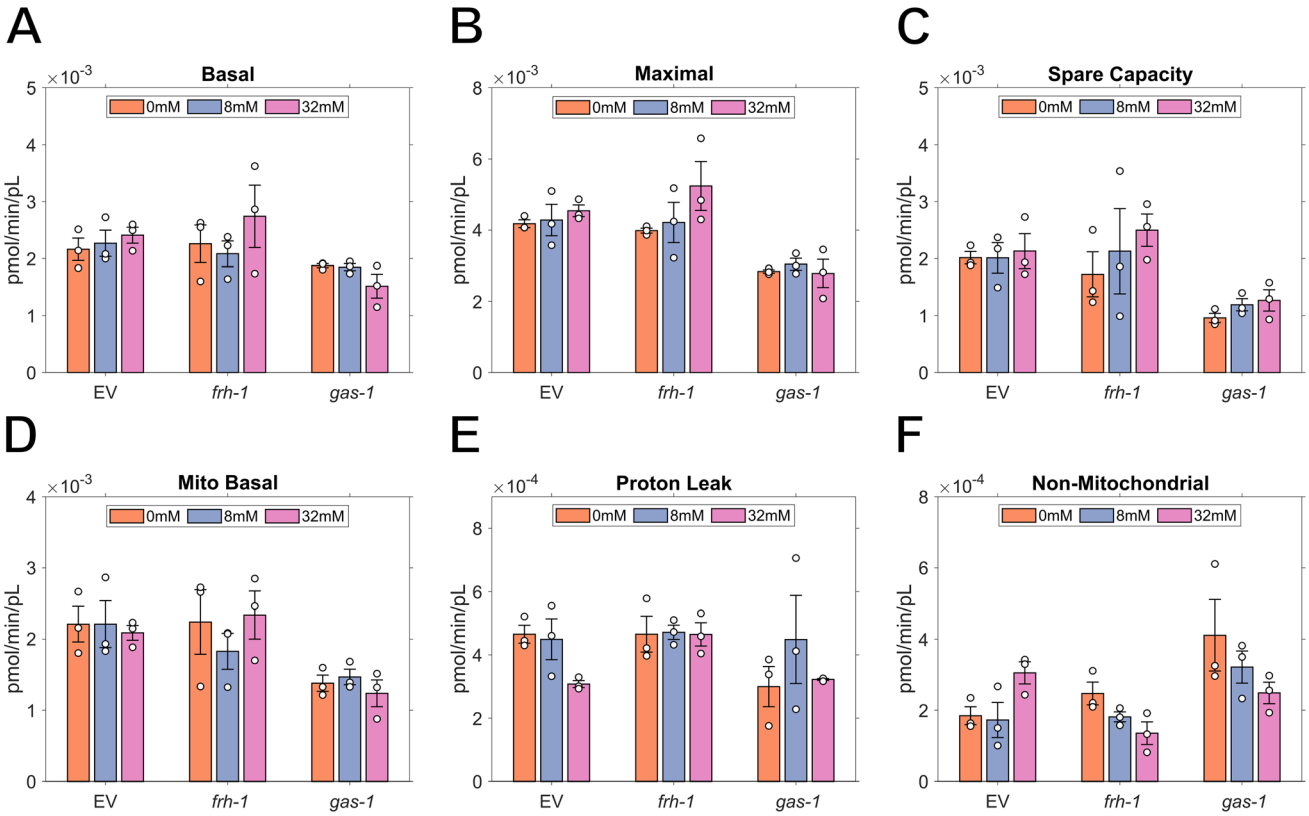

H

	Basal	Max.	Spare	Prt. Leak	Non-mito	MitoB
RNAi	0.021	< 0.001	0.004	0.114	0.005	0.002
LiNMC concentration	0.750	0.238	0.370	0.214	0.288	0.883
Interaction	0.386	0.402	0.897	0.418	0.054	0.670

I

	mtCN/nCN
RNAi	0.214
LiNMC concentration	0.615
Interaction	0.705

Fig. 4 OCR and mtDNA copy number are unaltered after exposure to LiNMC. Comparison of (A) basal OCR, (B) maximal OCR, (C) spare OCR capacity, (D) mitochondrial basal OCR, (E) proton leak, and (F) non-mitochondrial respiration between groups exposed to either 0, 8, or 32 mM LiNMC, and fed empty vector (EV), *frh-1* or *gas-1* RNAi bacteria. (G) Mitochondrial to nuclear DNA copy number ratio comparison for all groups. Summary of main effects of LiNMC and RNAi on (H) OCR and (I) mtDNA to nDNA copy number ratio. Two-way ANOVA with Tukey-HSD; error bars are SEM, $n = 3$ biological replicates (5 technical replicates per biological replicate, 20–30 L4 worms per technical replicate).

We reasoned that if the neurodegenerative effects observed were caused by lithium leaching from LiNMC, then we should be able to repeat these effects. However, we did not observe significant neurodegeneration in dopaminergic, glutamatergic, cholinergic, or GABAergic neurons after parental exposure to lithium chloride (Fig. 5H–K).

It may not be surprising that we did not see neurodevelopmental toxicity after lithium ion by itself. Several previous publications report neuroprotective effects of lithium in animal models, induction of developmental delays without developmental neurotoxicity, and the protection of cultured neurons from cell death induced by amyloid beta, a hallmark of Alzheimer's disease.[77–79] In contrast, developmental exposure to nickel using a *C. elegans* model revealed significant degeneration of dopaminergic, cholinergic, and GABAergic neurons, suggested to be linked to increased oxidative stress.[80] Similarly, reports indicate that manganese causes dopaminergic neurodegeneration in a *C. elegans* Parkinson's disease model,[81] and in mixtures with other heavy metals.[82] However, the effect of manganese was largely dopaminergic neuron-specific in the study by Benedetto *et al.*.[81] This suggests that the developmental neurotoxicity we observed in other neurons is unlikely to result only from the manganese, although it is also conceivable that the broader effects we saw were the result of a different exposure

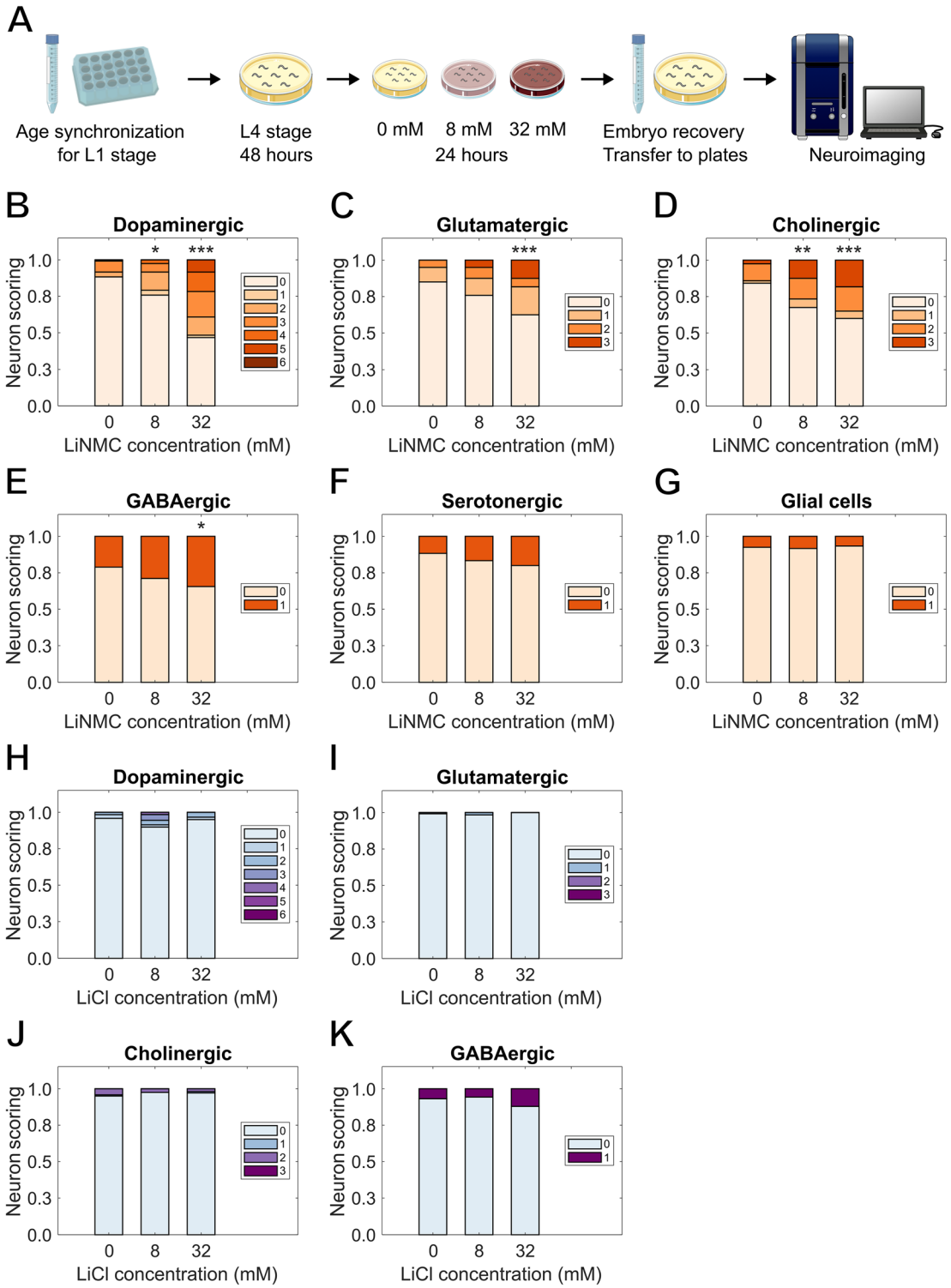

Fig. 5 Parental exposure to LiNMC causes neurodegeneration in progeny. (A) Parental (P0) worms were exposed to LiNMC for 24 hours after reaching the L4 larval stage, their progeny was recovered, and neurodegeneration in this F1 generation quantified at the L4 larval stage. Neurodegeneration scored for neuronal types (defined by neurotransmitter) after parental exposure to LiNMC: (B) dopaminergic, (C) glutamatergic, (D) cholinergic, (E) GABAergic, (F) serotonergic, and (G) glial cells. Neurodegeneration scored for neuronal types (defined by neurotransmitter) after parental exposure to lithium chloride: (H) dopaminergic, (I) glutamatergic, (J) cholinergic, and (K) GABAergic. Chi-square with Bonferroni correction, $n = 3$ biological replicates (20 worms per treatment), (*) $p < 0.05$, (**) $p < 0.01$, (***) $p < 0.001$.

paradigm that included more of neuronal development. Cobalt nanoparticles exposure in *C. elegans* caused alterations in acetylcholinesterase activity,[83] and mitochondrial dysfunction associated with neurodegeneration.[84] This suggests that the

observed neurodegeneration in certain types of neurons that we observed after exposure to LiNMC could be the result of exposure to one or a combination of more than one of the components of LiNMC.

The factors that determine differential sensitivity of different types of neurons are unclear. In many of the above-cited studies and others, neurodegeneration after exposures to these metals is attributed to an increase in oxidative stress and mitochondrial stress, with an increase in the response of antioxidant pathway genes *gst-4* and *skn-1*;[80,81] generation of reactive oxygen species with rescue enacted using the well-characterized antioxidant *N*-acetylcysteine;[83] induction of mitochondrial dysfunction by increased reactive oxygen species levels leading to ATP reduction and mitochondrial fragmentation.[84] Oxidative stress resulting from the generation of reactive oxygen species and disruption of ROS-metabolizing enzymes caused by the presence of some of these metallic elements[85,86] is often described as the potential cause for neurodegeneration. Different types of neurons could be more or less sensitive to oxidative stress or mitochondrial dysfunction if they were more vulnerable to oxidative or bioenergetic stress, or if there were significant toxicokinetic differences resulting in different levels of exposure. Alternatively, it is possible that it is not the individual components, but a particle-specific effect of LiNMCs that is causative of neurodegeneration in this work. Particle-specific effects include surface reactivity, as we discuss below, or characteristics such as shape. This is supported by the influence of the shape of ZnO particles on their neurotoxicity in a RSC96 Schwann cell model, with nanoparticles and microspheres having significant cytotoxic effects but no significant effects measured for prism-like and flower-like structures.[87]

4 Conclusions

Our hypothesis that LiNMCs would cause bioenergetic and redox stress, at least as assessed at the whole-organism level, were not supported by the exposure test results. A summary of trends of the effects of LiNMC exposure, broken down by RNAi type, for assays in this article are detailed in Table 1. LiNMCs did not significantly impact the redox state, steady-state ATP levels, mitochondrial : nuclear DNA ratio, or oxygen consumption in worms exposed developmentally to amounts of LiNMC that caused mild growth inhibition. Furthermore, while knockdown of *frh-1* and *gas-1* altered a number of parameters on their own, knockdown of these genes did not increase or decrease the effects of LiNMCs. This result further suggests that the LiNMC mechanism of organismal toxicity (in particular, growth inhibition) is something other than mitochondrial dysfunction or redox stress, because *gas-1* and *frh-1* worms are oxidative stress-sensitive[37,38] and bioenergetically challenged.[39,40]

Table 1 Summary of results for the effects of LiNMC in the context of RNAi treatments using various assays

Endpoint measured	Control RNAi	*frh-1* RNAi	*gas-1* RNAi
Length (redox state reporter)	↓	↓	↓
Redox state	=	=	=
Length (ATP reporter)	=	=	=
ATP	=	=	=
Oxygen consumption rate (overall)	=	=	=
mtDNA copy number	=	=	=
Neurodegeneration	↑	N/A	N/A

These results are intriguing, given that the literature described in the Introduction has suggested that both the individual components of LiNMCs and other Li-containing particles (LCOs) cause mitochondrial dysfunction and oxidative stress. This is particularly surprising in the context of a large body of literature from the Klaper group that has resulted in development of an adverse outcome pathway (AOP) for LCOs[28–32] beginning with reactive oxygen species and including metabolic disruption. Interestingly, the Carlson group's findings also support the proposed AOP with generation of reactive oxygen from LiNMC exposure and include different cascading effects like bacterial filamentation and DNA damage.[33,34] We do note some methodological differences that may contribute to our different results. The Klaper team measured direct Fe–S oxidation, which likely reports on oxidative damage *per se*, while we measured redox state of a roGFP protein coupled to glutathione reductase that reports largely on the redox state of cellular glutathione. It is also possible that there was oxidative stress in our experiments, but not at the time that we made measurements, or in a form or level that was not detected by our methodology, or only in certain areas. Future rescue experiments could help clarify this.

Another potentially important possibility is that the AOP for LCOs and the AOP for LiNMCs may simply differ in the mechanism of toxicity, although the authors suggest that LCO's proposed AOP could be broadly relevant to other transition metal oxide (TMO) LIB cathode nanomaterials,[32] and the Carlson group also reported generation of reactive oxygen species with LiNMC exposure.[33,34] However, the LiNMC we used is not defined as a nanomaterial (1 to 100 nm), as it has an average size of <500 nm. Nonetheless, LiNMC microparticles are commercially relevant,[88] and our work provides mechanistic insights on their toxicity, which is beneficial since they are widely used. We speculate that our results indicating a minor role for oxidative stress may be explained by given that we used larger particles, which have a significantly lower surface area : mass ratio than nano-sized Li particles used in those studies, and surface reactivity frequently mediates the degree to which particles cause toxicity by oxidative stress. Nanoparticles have a higher surface area : volume ratio and potentially greater surface reactivity and rate of dissolution on a molar basis. They also have a larger number of particles per equivalent mass, and likely more potential to be taken up by *C. elegans* compared to the equivalent mass of larger particles. For example, Liu *et al.*, found dissolution and skin permeation of nitrofurazone in nanoparticle-loaded gels was particle size dependent.[89] These differences could increase both the effective dose and toxic effect of nano-sized LiNMC particles in comparison to those we used; they may also change the mechanism of toxicity. Finally, *C. elegans* could have different biological responses than the

invertebrate species studied by other researchers such that the AOP is not the same. However, this seems relatively unlikely because worms are also invertebrates.

Our most interesting result was significant neurodegenerative effects of LiNMC in dopaminergic, glutamatergic, cholinergic, and GABAergic neurons. However, we could not detect neurodegeneration when exposing worms to lithium by itself. This, along with previous work showing neurodegeneration from individual components of LiNMCs suggests that the neurodegeneration is caused by one or a combination of the other metals in the LiNMCs. That is, the neurodegeneration we observed after LiNMC exposure likely results from the nickel, manganese, cobalt (that was present at particularly high internal levels), or a mixture of these, potentially in a particle-specific fashion. These results warrant further research to determine the mechanistic pathways involved in LiNMC-associated neurodegeneration. Notably, it is possible that redox stress or mitochondrial dysfunction were involved in neurodegeneration, as we did not assess these outcomes specifically in the neurons, and neuron-specific effects would not likely be picked up with our whole-organism assays. Efforts should also be made to estimate current and future human exposure to such particles, especially with usage increasing and in the context of poorly regulated disposal or burning of LiNMC batteries, because it is currently uncertain whether the amounts we used are (or might be in the future) environmentally relevant.

Additional future steps include understanding the mechanism of growth inhibition of the LiNMCs, assessing if the dissolution of LiNMC drives toxicity, and testing other LiNMC particle sizes to see if the mechanism depends on the LiNMC particle size.

Author contributions

RFL: conceptualization, data curation, formal analysis, investigation, methodology, visualization, writing – original draft, writing – review & editing. JH: conceptualization, data curation, formal analysis, investigation, methodology, visualization, writing – original draft, writing – review & editing. GDZW: formal analysis, investigation, methodology, writing – original draft. SAS: formal analysis, investigation. PDL: writing – original draft, writing – review & editing. SNB: investigation. AV: funding acquisition, resources, supervision, writing – review &editing. JM: conceptualization, funding acquisition, project administration, resources, supervision, writing – original draft, writing – review &editing.

Conflicts of interest

No conflicts of interest to declare.

Data availability

Data for this article are available at Duke University Digital Repository at **https://doi.org/10.7924/r4kk9js30**.

Supplementary information is available. See DOI: **https://doi.org/10.1039/d5va00103j**.

Acknowledgements

This work was funded by NIH grant R01ES034270. Some strains were provided by the CGC, which is funded by NIH Office of Research Infrastructure Programs (P40 OD010440). Research reported in this manuscript was supported by NIEHS under award number P42 ES010356. The content is solely the responsibility of the authors and does not necessarily represent the official views of the National Institutes of Health. c-elegans_small_mutant icon, plate-reader icon, and desktop_electron_microscope icon by DBCLS **https://togotv.dbcls.jp/en/pics.html** are licensed under CC-BY 4.0; petri-dish-yellow icon, falcon-15ml-empty icon, and petri-dish-brown icon by Servier **https://smart.servier.com/** are licensed under CC-BY 3.0.

References

1 X. Lai, H. Gu, Q. Chen, X. Tang, Y. Zhou, F. Gao, X. Han, Y. Guo, R. Bhagat and Y. Zheng, *J. Clean. Prod.*, 2022, **372**, 133756.
2 F. Wang, C. Intrator, N. Salopek and C. Yuan, *Proced. CIRP*, 2022, **105**, 489–494.
3 V. Pimenta, M. Sathiya, D. Batuk, A. M. Abakumov, D. Giaume, S. Cassaignon, D. Larcher and J.-M. Tarascon, *Chem. Mater.*, 2017, **29**, 9923–9936.
4 A. Marashli, A. I. Al-Kassab, D. M. Gab-Allah, M. Shalby and A. Salah, *Results Eng.*, 2024, **23**, 102489.
5 X. Yang, H. Wen, Y. Liu, Y. Huang, Q. Zhang, W. Wang, H. Zhang, J. Fu, G. Li, Q. Liu and G. Jiang, *Environ. Sci. Technol.*, 2024, **58**, 11637–11648.
6 G. D. Z. Williams and A. Vengosh, *Environ. Sci. Technol. Lett.*, 2025, **12**, 151–157.
7 G. D. Z. Williams, S. Saltman, Z. Wang, D. M. Warren, R. C. Hill and A. Vengosh, *Sci. Total Environ.*, 2024, **956**, 177281.
8 S. Natarajan and V. Aravindan, *Adv. Energy Mater.*, 2020, **10**, 2002238.
9 W. Mrozik, M. A. Rajaeifar, O. Heidrich and P. Christensen, *Energy Environ. Sci.*, 2021, **14**, 6099–6121.
10 E. M. Melchor-Martínez, R. Macias-Garbett, A. Malacara-Becerra, H. M. N. Iqbal, J. E. Sosa-Hernández and R. Parra-Saldívar, *Case Stud. Chem. Environ. Eng.*, 2021, **3**, 100104.
11 R. W. Licht, *CNS Neurosci. Ther.*, 2012, **18**, 219–226.
12 B. Kores and M. H. Lader, *Clin. Neuropharmacol.*, 1997, **20**, 283–299.
13 S. Gentile, *Expet Opin. Drug Saf.*, 2012, **11**, 425–437.
14 C. Kozma, *Am. J. Med. Genet., Part A*, 2005, **132A**, 441–444.
15 N. M. van der Lugt, J. S. van de Maat, I. L. van Kamp, E. A. M. Knoppert-van der Klein, J. G. F. M. Hovens and F. J. Walther, *Early Hum. Dev.*, 2012, **88**, 375–378.
16 E. M. P. Poels, L. Schrijver, A. M. Kamperman, M. H. J. Hillegers, W. J. G. Hoogendijk, S. A. Kushner and S. J. Roza, *Eur. Child Adolesc. Psychiatr.*, 2018, **27**, 1209–1230.

17 M. S. Allagui, C. Vincent, A. El feki, Y. Gaubin and F. Croute, *Biochim. Biophys. Acta*, 2007, **1773**, 1107–1115.
18 M. Shabani, Z. Jamali, D. Bayrami and A. Salimi, *Drug Chem. Toxicol.*, 2024, **47**, 597–605.
19 B. Adkins, J. H. Richards and D. E. Gardner, *Environ. Res.*, 1979, **20**, 33–42.
20 J. Cheek, S. S. Fox, H.-J. Lehmler and T. J. Titcomb, *Expo. Health*, 2023, **16**, 1–9.
21 Y. Nan, J. Yang, L. Ma, L. Jin and Y. Bai, *J. Trace Elem. Med. Biol.*, 2022, **74**, 127065.
22 A. W. Dobson, K. M. Erikson and M. Aschner, *Ann. N. Y. Acad. Sci.*, 2004, **1012**, 115–128.
23 D. Budinger, S. Barral, A. K. S. Soo and M. A. Kurian, *Lancet Neurol.*, 2021, **20**, 956–968.
24 M. R. Smith, J. Fernandes, Y.-M. Go and D. P. Jones, *Biochem. Biophys. Res. Commun.*, 2017, **482**, 388–398.
25 J. D. Crowley, D. A. Traynor and D. C. Weatherburn, *Met. Ions Biol. Syst.*, 2000, **37**, 209–278.
26 M. Jiang, K. Wang, Y. Wang, Q. Zhao and W. Wang, *Sci. Total Environ.*, 2022, **813**, 151908.
27 V. Battaglia, A. Compagnone, A. Bandino, M. Bragadin, C. A. Rossi, F. Zanetti, S. Colombatto, M. A. Grillo and A. Toninello, *Int. J. Biochem. Cell Biol.*, 2009, **41**, 586–594.
28 J. Bozich, M. Hang, R. Hamers and R. Klaper, *Environ. Toxicol. Chem.*, 2017, **36**, 2493–2502.
29 N. J. Niemuth, B. J. Curtis, M. N. Hang, M. J. Gallagher, D. H. Fairbrother, R. J. Hamers and R. D. Klaper, *Environ. Sci. Technol.*, 2019, **53**, 3860–3870.
30 B. J. Curtis, N. J. Niemuth, E. Bennett, A. Schmoldt, O. Mueller, A. A. Mohaimani, E. D. Laudadio, Y. Shen, J. C. White, R. J. Hamers and R. D. Klaper, *Nat. Nanotechnol.*, 2022, **17**, 661–669.
31 N. J. Niemuth, B. J. Curtis, E. D. Laudadio, E. Sostare, E. A. Bennett, N. J. Neureuther, A. A. Mohaimani, A. Schmoldt, E. D. Ostovich, M. R. Viant, R. J. Hamers and R. D. Klaper, *Chem. Res. Toxicol.*, 2021, **34**, 2287–2297.
32 N. J. Niemuth, Y. Zhang, A. A. Mohaimani, A. Schmoldt, E. D. Laudadio, R. J. Hamers and R. D. Klaper, *Environ. Sci. Technol.*, 2020, **54**, 15257–15266.
33 D. Sharan, D. Wolfson, C. M. Green, P. Lemke, A. G. Gavin, R. J. Hamers, Z. V. Feng and E. E. Carlson, *Environ. Sci. Nano*, 2023, **10**, 1978–1992.
34 S. L. Mitchell, N. V. Hudson-Smith, D. Sharan, C. L. Haynes and E. E. Carlson, *Environ. Sci. Nano*, 2024, **11**, 483–493.
35 M. N. Hang, I. L. Gunsolus, H. Wayland, E. S. Melby, A. C. Mensch, K. R. Hurley, J. A. Pedersen, C. L. Haynes and R. J. Hamers, *Chem. Mater.*, 2016, **28**, 1092–1100.
36 J. Wang, X. Fang, R. Wu, Z. Liu, G. Wang, Y. Hu, H. Wang, J. Pi and Y. Xu, *Toxicology*, 2025, **511**, 154036.
37 M. Kondo, N. Senoo-Matsuda, S. Yanase, T. Ishii, P. S. Hartman and N. Ishii, *Mech. Ageing Dev.*, 2005, **126**, 637–641.
38 R. P. Vázquez-Manrique, P. González-Cabo, S. Ros, H. Aziz, H. A. Baylis and F. Palau, *FASEB J.*, 2006, **20**, 172–174.
39 E. B. Kayser, P. G. Morgan, C. L. Hoppel and M. M. Sedensky, *J. Biol. Chem.*, 2001, **276**, 20551–20558.
40 K. Zarse, T. J. Schulz, M. Birringer and M. Ristow, *FASEB J.*, 2007, **21**, 1271–1275.
41 M. C. K. Leung, P. L. Williams, A. Benedetto, C. Au, K. J. Helmcke, M. Aschner and J. N. Meyer, *Toxicol. Sci.*, 2008, **106**, 5–28.
42 L. L. Maurer, I. T. Ryde, X. Yang and J. N. Meyer, *Curr. Protoc. Toxicol.*, 2015, **66**, 1–25.
43 L. L. Maurer, A. L. Luz and J. N. Meyer in *Mitochondrial Dysfunction Caused by Drugs and Environmental Toxicants*, Wiley, 2018, vol. 2–2, pp. 655–689.
44 J. A. Ruszkiewicz, A. Pinkas, M. R. Miah, R. L. Weitz, M. J. A. Lawes, A. J. Akinyemi, O. M. Ijomone and M. Aschner, *Toxicol. Appl. Pharmacol.*, 2018, **354**, 126–135.
45 P. L. Williams and D. B. Dusenbery, *Toxicol. Ind. Health*, 1988, **4**, 469–478.
46 T. Stiernagle, *WormBook*, 2006, pp. 1–11.
47 L. Byerly, R. C. Cassada and R. L. Russell, *Dev. Biol.*, 1976, **51**, 23–33.
48 R. S. Kamath and J. Ahringer, *Methods*, 2003, **30**, 313–321.
49 M. Porta-de-la-Riva, L. Fontrodona, A. Villanueva and J. Cerón, *J. Vis. Exp.*, 2012, (64), 4019.
50 S. R. Bijwadia, K. Morton and J. N. Meyer, *J. Vis. Exp.*, 2021, (177), DOI: **10.3791/62894**.
51 J. Huayta, S. Seay, J. Laster, N. A. Rivera, A. S. Joyce, P. L. Ferguson, H. Hsu-Kim and J. N. Meyer, *ALTEX*, 2025, DOI: **10.14573/altex.2501151**.
52 B. T. Moore, J. M. Jordan and L. R. Baugh, *PLoS One*, 2013, **8**, e57142.
53 A. Luz, C. Lagido, M. D. Hirschey and J. N. Meyer, *Curr. Protoc. Toxicol.*, 2016, **69**, 25.28.21–25.28.22.
54 D. F. Mello, L. Perez, C. M. Bergemann, K. S. Morton, I. T. Ryde and J. N. Meyer, *PLoS One*, 2024, **19**, e0306849.
55 T. C. Leuthner, J. H. Hartman, I. T. Ryde and J. N. Meyer, *Methods Mol. Biol.*, 2021, **2310**, 91–111.
56 J. H. Hartman, S. J. Widmayer, C. M. Bergemann, D. E. King, K. S. Morton, R. F. Romersi, L. E. Jameson, M. C. K. Leung, E. C. Andersen, S. Taubert and J. N. Meyer, *J. Toxicol. Environ. Health B Crit. Rev.*, 2021, **24**, 51–94.
57 K.-P. Chen, W. W. Shen and M.-L. Lu, *Psychiatr. Clin. Neurosci.*, 2004, **58**, 25–29.
58 A. Jaeger, P. Sauder, J. Kopferschmitt, L. Tritsch and F. Flesch, *J. Toxicol. Clin. Toxicol.*, 1993, **31**, 429–447.
59 T. A. Demir, B. Işikli, S. M. Urer, A. Berber, T. Akar, M. Canbek and C. Kalyoncu, *BioMetals*, 2005, **18**, 7–13.
60 F. W. Sunderman, B. Dingle, S. M. Hopfer and T. Swift, *Am. J. Ind. Med.*, 1988, **14**, 257–266.
61 E. Pefferkorn, B. Clément, A. Bascou, C. Guilbeau-Frugier, N. Telmon, F. Savall and F. Dedouit, *Forensic Sci. Med. Pathol.*, 2024, **21**(1), 295–301.
62 A. Woolf, R. Wright, C. Amarasiriwardena and D. Bellinger, *Environ. Health Perspect.*, 2002, **110**, 613–616.
63 X. G. Kondakis, N. Makris, M. Leotsinidis, M. Prinou and T. Papapetropoulos, *Arch. Environ. Health*, 1989, **44**, 175–178.
64 J. Xiao, Q. Rui, Y. Guo, X. Chang and D. Wang, *J. Environ. Sci.*, 2009, **21**, 842–848.

65 P. Gubert, B. Puntel, T. Lehmen, J. P. Fessel, P. Cheng, J. Bornhorst, L. S. Trindade, D. S. Avila, M. Aschner and F. A. A. Soares, *Neurotoxicology*, 2018, **67**, 65–72.
66 C. Au, A. Benedetto, J. Anderson, A. Labrousse, K. Erikson, J. J. Ewbank and M. Aschner, *PLoS One*, 2009, **4**, e7792.
67 Y. Ichikawa, Y. Kusaka and S. Goto, *Int. Arch. Occup. Environ. Health*, 1985, **55**, 269–276.
68 B. E. Tvermoes, K. M. Unice, D. J. Paustenbach, B. L. Finley, J. M. Otani and D. A. Galbraith, *Am. J. Clin. Nutr.*, 2014, **99**, 632–646.
69 M. D. Brand and D. G. Nicholls, *Biochem. J.*, 2011, **435**, 297–312.
70 S. S. Vergano, M. Rao, S. McCormack, J. Ostrovsky, C. Clarke, J. Preston, M. J. Bennett, M. Yudkoff, R. Xiao and M. J. Falk, *Mol. Genet. Metab.*, 2014, **111**, 331–341.
71 B. G. Janssen, E. Munters, N. Pieters, K. Smeets, B. Cox, A. Cuypers, F. Fierens, J. Penders, J. Vangronsveld, W. Gyselaers and T. S. Nawrot, *Environ. Health Perspect.*, 2012, **120**, 1346–1352.
72 J. L. Fetterman, M. Pompilius, D. G. Westbrook, D. Uyeminami, J. Brown, K. E. Pinkerton and S. W. Ballinger, *PLoS One*, 2013, **8**, e66835.
73 S. Pavanello, L. Dioni, M. Hoxha, U. Fedeli, D. Mielzynska-Svach and A. A. Baccarelli, *Cancer Epidemiol. Biomarkers Prev.*, 2013, **22**, 1722–1729.
74 J. N. Meyer, T. C. Leuthner and A. L. Luz, *Toxicology*, 2017, **391**, 42–53.
75 C. P. Gonzalez-Hunt, J. P. Rooney, I. T. Ryde, C. Anbalagan, R. Joglekar and J. N. Meyer, *Curr. Protoc. Toxicol.*, 2016, **67**, 1–25.
76 E. Area-Gomez, C. Guardia-Laguarta, E. A. Schon and S. Przedborski, *J. Clin. Invest.*, 2019, **129**, 34–45.
77 G. Alvarez, J. R. Muñoz-Montaño, J. Satrústegui, J. Avila, E. Bogónez and J. Díaz-Nido, *FEBS Lett.*, 1999, **453**, 260–264.
78 M. Bauer, M. Alda, J. Priller, L. T. Young and International Group For The Study Of Lithium Treated Patients (IGSLI), *Pharmacopsychiatry*, 2003, **36**(3), S250–S254.
79 P. R. Hunt, N. Olejnik, K. D. Bailey, C. A. Vaught and R. L. Sprando, *Food Chem. Toxicol.*, 2018, **121**, 583–592.
80 O. M. Ijomone, M. R. Miah, G. T. Akingbade, H. Bucinca and M. Aschner, *Neurotox. Res.*, 2020, **37**, 1018–1028.
81 A. Benedetto, C. Au, D. S. Avila, D. Milatovic and M. Aschner, *PLoS Genet.*, 2010, **6**, e1001084.
82 B. Tang, P. Tong, K. S. Xue, P. L. Williams, J.-S. Wang and L. Tang, *Chemosphere*, 2019, **234**, 232–241.
83 C. Chen, J. Chen, X. Lin, J. Yang, H. Qu, L. Li, D. Zhang, W. Wang, X. Chang, Z. Guo, P. Cai, G. Yu, W. Shao, H. Hu, S. Wu, H. Li, J. Bornhorst, M. Aschner and F. Zheng, *Toxicol. Sci.*, 2023, **196**, 85–98.
84 J. Chen, C. Chen, N. Wang, C. Wang, Z. Gong, J. Du, H. Lai, X. Lin, W. Wang, X. Chang, M. Aschner, Z. Guo, S. Wu, H. Li and F. Zheng, *Neurotoxicology*, 2023, **95**, 155–163.
85 V. M. Andrade, M. L. Mateus, M. C. Batoréu, M. Aschner and A. P. Marreilha dos Santos, *Biol. Trace Elem. Res.*, 2015, **166**, 13–23.
86 P. Chen, M. R. Miah and M. Aschner, *F1000Research*, 2016, **5**, 366.
87 Y. Yin, Q. Lin, H. Sun, D. Chen, Q. Wu, X. Chen and S. Li, *Nanoscale Res. Lett.*, 2012, **7**, 439.
88 P.-C. Tsai, B. Wen, M. Wolfman, M.-J. Choe, M. S. Pan, L. Su, K. Thornton, J. Cabana and Y.-M. Chiang, *Energy Environ. Sci.*, 2018, **11**, 860–871.
89 X. Liu, B. Shen, C. Shen, R. Zhong, X. Wang and H. Yuan, *J. Drug Deliv. Sci. Technol.*, 2018, **45**, 367–372.